



# Comprehensive insight into mercury contamination in atmospheric, terrestrial and aquatic ecosystems surrounding a typical antimony-coal mining district

Lulu Mao<sup>a</sup>, Wenbo Ren<sup>a</sup>, Yang Tang<sup>b</sup>, Xitao Liu<sup>a,\*</sup>, Mengchang He<sup>a</sup>, Ke Sun<sup>a</sup>, Bo-Tao Zhang<sup>c</sup>, Chunye Lin<sup>a</sup>, Wei Ouyang<sup>a,d</sup>

<sup>a</sup> State Key Laboratory of Water Environment Simulation, School of Environment, Beijing Normal University, Beijing 100875, China

<sup>b</sup> State Key Laboratory of Ore Deposit Geochemistry, Institute of Geochemistry, Chinese Academy of Sciences, 550081 Guiyang, China

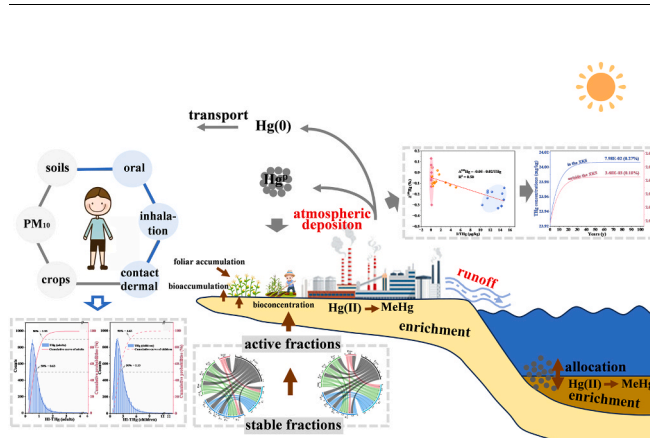
<sup>c</sup> College of Water Sciences, Beijing Normal University, Beijing 100875, China

<sup>d</sup> Advanced Interdisciplinary Institute of Environment and Ecology, Beijing Normal University, Zhuhai 519087, China

## HIGHLIGHTS

- Multiple environment media in an antimony-coal mining area were contaminated with Hg.
- Considerable Hg deposition flux ( $3.12 \pm 2.20 \text{ mg/m}^2/\text{y}$ ) was found in the XKS.
- Atmospheric deposition dominated Hg contamination on surface soils in the XKS.
- Compared with soils, sediments presented higher static and dynamic Hg risks.
- Consuming leaf vegetables posed high THg risk for local residents.

## GRAPHICAL ABSTRACT



## ARTICLE INFO

### Keywords:

Hg isotope signatures, binary mixing model  
DGH model  
Monte Carlo simulation

## ABSTRACT

This study comprehensively investigated mercury (Hg) contents of various environmental compartments in a typical antimony-coal mining area with intensive industrial activities over the past 120 years to analyze Hg environmental behaviors and evaluate Hg risks. The total mercury (THg) contents in river water, sediments, soils, PM<sub>10</sub>, dust falls, vegetables and corns were  $1.16 \pm 0.63 \text{ }\mu\text{g/L}$ ,  $2.01 \pm 1.64 \text{ mg/kg}$ ,  $1.87 \pm 3.88 \text{ mg/kg}$ ,  $7.87 \pm 18.68 \text{ ng/m}^3$ ,  $13.01 \pm 14.53 \text{ mg/kg}$ ,  $0.30 \pm 0.34 \text{ mg/kg}$  and  $3.11 \pm 0.51 \text{ }\mu\text{g/kg}$ , respectively. The  $\delta^{202}\text{Hg}$  values in soils and dust falls were  $-1.58 \sim 0.12\text{‰}$  and  $0.25 \sim 0.30\text{‰}$ , respectively. Environmental samples affected by industrial activities in the Xikuangshan (XKS) presented higher THg and  $\delta^{202}\text{Hg}$  values. Binary mixing model proved that atmospheric deposition with considerable Hg deposition flux ( $0.44 \sim 6.40$ ,  $3.12 \pm 2.20 \text{ mg/m}^2/\text{y}$ ) in the XKS significantly contributed to Hg accumulations on surface soils. Compared with soils, sediments with more frequent paths and higher burst probabilities presented higher dynamic Hg risks. Children were faced

\* Corresponding author.

E-mail address: [liuxt@bnu.edu.cn](mailto:liuxt@bnu.edu.cn) (X. Liu).

<https://doi.org/10.1016/j.jhazmat.2024.133880>

Received 5 December 2023; Received in revised form 27 January 2024; Accepted 22 February 2024

Available online 23 February 2024

0304-3894/© 2024 Elsevier B.V. All rights reserved.

higher health risk of multiple Hg exposure than adults. Furthermore, the health risk of THg by consuming leaf vegetables deserved more attention. These findings provided scientific basis for managing Hg contamination.

### 1. Introduction

Mercury (Hg), with high persistence, toxicity and bioavailability [24], has been regarded as a top ten chemical in public health concern by World Health Organization (WHO) [43]. Methylmercury (MeHg), the organic form of Hg, has the highest toxicity and risk [25]. The Hg released from natural processes [10] and anthropogenic activities [15] enters the adjacent ecosystems mainly through river transportation [39] and atmospheric deposition [34], causing severe Hg contamination in the environment, further resulting in potential Hg risks faced by populations. Furthermore, the emitted Hg from non-ferrous metals mining and smelting constitutes the vital proportions (15%) [37] of anthropogenic Hg emissions and has been widely concerned [27,41].

China's production, consumption and trade of non-ferrous metals rank first in the world [54], resulting the Hg contamination caused by non-ferrous industries has been widely reported, such as Hg mining and smelting area in Tongren, Guizhou Province [46], Au mining area in Huadian, Jilin Province [41], Pb/Zn smelter area in Zhuzhou, Hunan Province [19,18], Sb mining and smelting area in Lengshuijiang, Hunan Province [7], and Cu mining area in Fuyang, Zhejiang Province [48]. However, these studies only focused on Hg contamination in a single medium or a few media in the studied area. During the mining and smelting of non-ferrous metals, the discharged wastewater carrying Hg was released to nearby aquatic ecosystems [11], the flue gas enriched with Hg unremoved completely by purification facilities was transmitted to surrounding aquatic and terrestrial ecosystems by atmospheric

deposition [15], resulting in Hg contamination in water, sediments, air, soils, plants, and organisms. Therefore, comprehensive focusing on various environmental media is crucial for fully revealing the Hg contamination in study areas.

Xikuangshan (XKS) situates in a low-temperature mineralization depression and contains resources such as non-ferrous metals (Sb, Hg, Au, Zn, Pb, As) and coal [8]. The Sb production of XKS accounted for 80% of Hunan Province, referred as "the Capital of Antimony" [4,42]. In addition, coal mining industry is distributed in the region [26]. The Lianxi River, originates from the XKS area, receives the mining and smelting drainage and flows into the Zijiang River [40]. Although Fu et al. [7] reported the Hg contents in water and fish in the XKS, the Hg contamination in other environment media and ecological and health risks caused by Hg contamination in the XKS need to be further revealed. The exhaust gas containing Hg emitted by Sb mining and smelting activities would be volatilized into the atmosphere and deposited onto the adjacent soils. However, the relative contribution of atmospheric Hg deposition from anthropogenic activities to the Hg accumulations in soils in the XKS has not been quantitatively evaluated. Hg isotope compositions has been widely used to track the Hg sources in contaminated soils [34,9]. Mixing model based on the mass dependent fractionation (MDF) and mass independent fractionation (MIF) has been widely used to trace multiple Hg sources in environmental samples and quantify relative proportions ([47,6]; Sun et al., 2020).

Some studies regarding risk assessment of heavy metal in solid phases were based on the static risk of THg concentrations [44] and

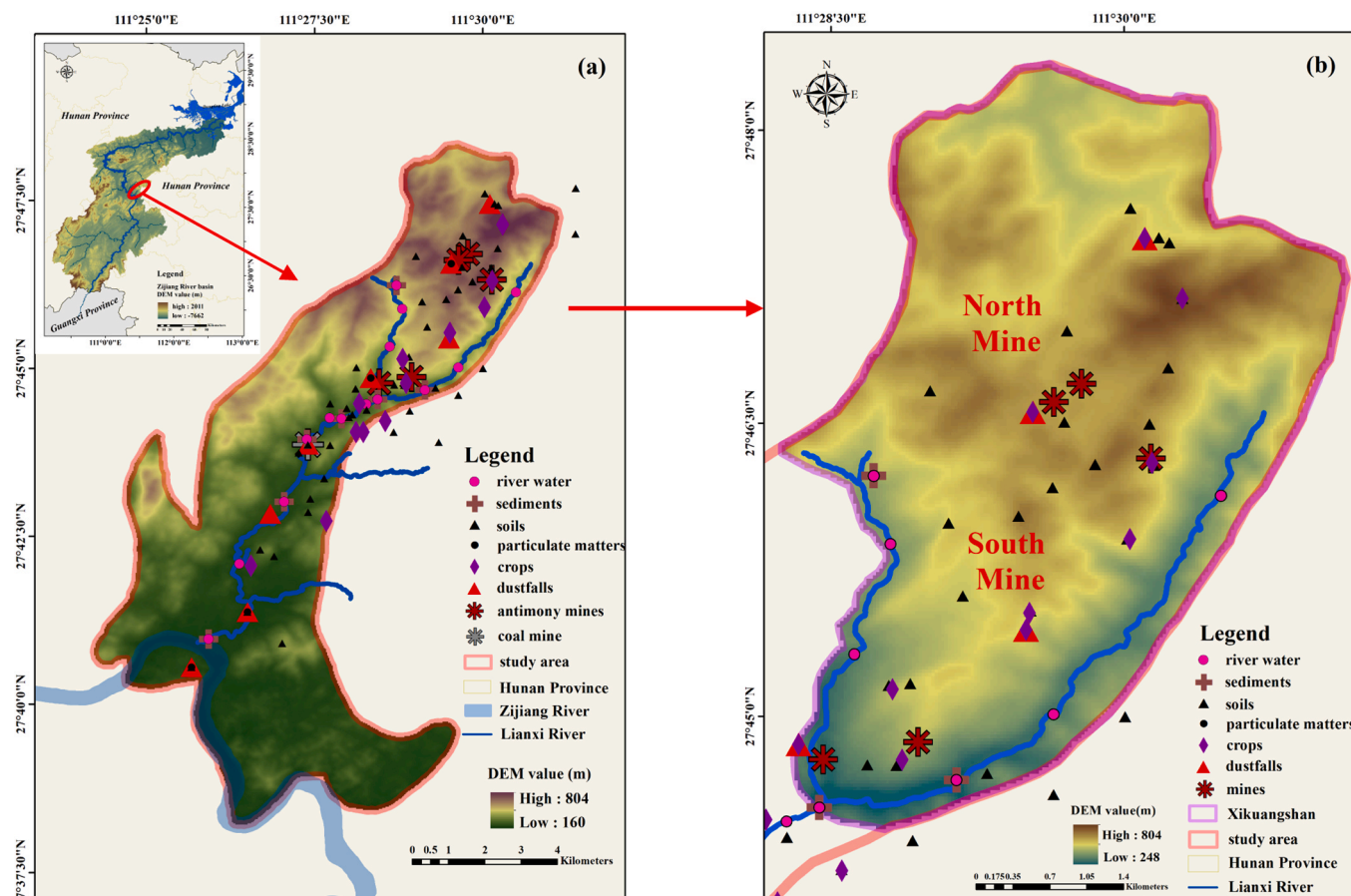


Fig. 1. The geographic locations of collected samples in the antimony-coal mine area (a) and the XKS (b).

active fractions proportions [29]. However, the continuous Hg input might cause Hg accumulation in environment, trigger the Delayed Geochemical Hazard (DGH) processes in soils and sediments, lead to the migration and transformation of Hg fractions and ultimately induce the dynamic Hg risks in environment [53]. Long term exposure to different environmental media (i.e., water, soils, air, crops and organisms) in Hg contaminated sites via multiple pathways (ingestion, dermal contact and inhalation) might cause potential hazards to populations [16,52]. Thus, residents near contaminated regions might face higher Hg exposure risks than general populations [1]. However, generic health risk assessment methods were limited by complexity of studied systems and variability of exposure parameters, resulting in high uncertainty of the results [31]. Monte Carlo simulation could predict the probabilistic risk distribution, quantify the uncertainty of risk evaluation and provide the information on population percentages in a specific range of hazard quotients [13, 14], thus was adopted to evaluate the health risks to inhabitants.

The primary aims were to: 1) determine Hg contamination and characterize Hg spatial distribution in various environmental media (river water, sediments, soils, atmospheric particulate matters (PM<sub>10</sub> and dust falls), crops (vegetables and corns)) in the region; 2) analyze the allocation, enrichment and transfer of Hg; 3) estimate the contribution of atmospheric Hg deposition on surface soils; 4) reveal the dynamic risk development paths and burst probabilities of Hg in sediments and soils; 5) quantitatively assess the health risks of multiple Hg exposure faced by local residents.

## 2. Materials and methods

### 2.1. Studied area description

The studied antimony-coal mine area with a total area of 80 km<sup>2</sup>, including the XKS and its surrounding area, locates in the midstream of the Zijiang River Basin and central part of Hunan Province, China (Fig. 1a). The XKS deposit covers 16 km<sup>2</sup> (Fig. 1b), including North Mine and South Mine. XKS antimony mine, referred as “the Capital of Antimony”, is a super large antimony mine with reserve of 859300 tons. Currently, the North Mine is smelting area, and the South Mine is mining area. The Tangchong coal mine is located between the XKS and the Lengshuijiang City. Apart from lands using for mining, most of lands are extensively applied for cultivation, mainly corns and vegetables. The Lianxi River flows through the XKS and the Tangchong coal mine, then injects into the Zijiang River at 14 km downstream of the XKS. Fu et al. [7] reported the Sb, As and Hg contamination in the Lianxi River. According to practical survey of local residents, the Lianxi River was not used for irrigation due to heavy metals pollution [7]. The XKS has been mined for more than 120 years [42], resulting the principal anthropogenic source of heavy metals to local environment.

### 2.2. Sampling and pretreatment

Surface river water samples (n = 29) within 14 km downstream of the smelters in North Mine were collected into 10% (V/V) nitric acid pretreated clean polyethylene plastic bottles and then acidified to pH < 2 in November 2020, April 2021 and July 2023. The unfiltered samples and filtered samples (0.45 μm Teflon membranes) were used to detect the total mercury (THg), dissolved Hg (DHg) and dissolved MeHg (DMeHg) contents in river water, respectively. The particulate Hg (PHg) contents were calculated by the difference between THg and DHg in river water.

Surface sediment samples (n = 17) corresponding to the river water samples (no sediment samples in some locations) were collected into polyethylene plastic bags in November 2020, April 2021 and July 2023. Pore water samples (n = 9) were extracted from collected sediments by centrifugation (3500 rpm, 10 min), and then filtered (0.45 μm) to remove particles to determine the DHg and DMeHg contents in pore water. Surface soil samples (n = 64) were collected with spades into

polyethylene plastic bags in October 2022 and April 2023. Soil profiles were collected from outside the XKS, and soil samples from the lower layer (below 100 cm) were selected to represent the local background soil. All collected soil samples are farmland soil, then litter and root mat were removed from the collected soil samples. In addition, no accumulated slag near the soil samples were found. Tuber vegetables (potato, sweet potato, carrot and garlic) (n = 32), leaf vegetables (head lettuce, cabbage and spinach) (n = 28) and corns (n = 9) in the mature period were collected at the distance of – 2 km (2 km upstream), – 0.5 km (0.5 km upstream), 2.5 km, 4 km, 7 km, 9 km, 10 km, 12 km and 14 km from the smelters in North Mine in October 2022 and April 2023, cleaned with deionized water and dissected the aboveground tissues and underground tissues of the entire plants. The solid samples and plant tissues were freeze-dried at – 40 °C, then grounded, passed through 200 mesh and stored at – 4 °C.

Particulate matter samples (n = 36) in atmosphere (PM<sub>2.5</sub> and PM<sub>10</sub>) were collected on constant-weighted quart fiber membranes (Pallflex Tissuquartz TM, 90 mm, USA) by medium volume air samplers (TH-150 C, Wuhan Tianhong Instruments Co., Ltd., China) for 24 h with flow rate of 100 L/min. The PM<sub>2.5</sub> and PM<sub>10</sub> samples were collected at the distance of – 0.5 km, 4 km, 11 km and 14 km from the smelters in North Mine in April 24–26, 2023 and July 19–20, 2023. Sized-fractioned particulates (<0.43 μm, 0.43–0.65 μm, 0.65–1.1 μm, 1.1–2.1 μm, 2.1–3.3 μm, 3.3–4.7 μm, 4.7–5.8 μm, 5.8–9.0 μm, 9.0–10 μm) (n = 3) were collected on constant-weighted quart filters (Thermo-Electron Co., USA) by a nine-stage cascade impactor (Anderson Series 20–800, USA) for 48 h with flow rate of 28.3 L/min. The segregated particles were collected at the front door of smelters, approximately 500 m away from the stack in the North Mine, in April 24–25, 2023 and July 19–20, 2023. After sampling, all filters were placed in a constant temperature and humidity chamber until the weigh precision of 10 μg, then was stored at – 4 °C.

Dust fall samples (n = 16), the mixing of dry and wet deposition, were obtained in cylindrical shape glass jars (15 cm × 30 cm) at the distance of – 2 km, 0 km, 2.5 km, 4 km, 7 km, 9 km, 12 km and 14 km from the smelters in North Mine from April 24, 2023 to July 20, 2023 and July 21, 2023 to November 08, 2023. The containers were fixed with iron wire and stainless steel meshes at the height of 2 m from the ground. The dust falls removed debris were transferred to glass beakers, dried at 80 °C to constant weight, then stored at – 4 °C.

### 2.3. Analysis methods

#### 2.3.1. THg analysis

The THg contents in the collected environmental samples were analyzed with a Direct Mercury Analyzer (DMA-80, Milestone, Italy). In brief, THg and DHg contents in water samples were analyzed with 1 mL and 2 mL samples by “concentrated function”, respectively. The recovery rates of Hg in the water samples were analyzed by the addition of certified material (GSB04–1729–2004, National Institute of Metrology), ranging from 82.24% to 96.17%. The coefficient variations (CVs) varied from 4.73% to 11.83%. Based on accumulated injection volume of 2 mL water samples, the detection limit (DL) of Hg was 6.50 ng/L. About 0.1 g soils, 0.1 g sediments, 0.05 g dust fall samples, 0.05 g vegetable samples and 0.05 g corn samples were placed into the nickel-made boats for THg detection. Four cut small circles (0.562 cm<sup>2</sup>) were evenly picked from the membrane for collecting particulate matter, then placed into the boats for THg detection. The recovery rates of THg in certified material (GBW08308), with the concentration of 0.48 ± 0.03 μg/g Hg in lake sediments, were stable (91.75% ~ 98.26%), and the CVs of the duplicate samples were low (2.30% ~ 6.50%). Based on 0.1 g solid samples, the detection limit (DL) of THg was 0.10 μg/kg.

#### 2.3.2. Hg speciation analysis

The MeHg contents in the collected environmental samples were quantified with a Fully Automatic Alkyl Mercury Analyzer (MMA72,

POLYTECH, China). The analysis method of dissolved MeHg (DMeHg) in river water is detailed in Text S1. Briefly, 25 mL distilled water samples, 30  $\mu\text{L}$   $\text{CH}_3\text{COOH}\text{-CH}_3\text{COONa}$  ( $\text{pH} = 4.6$ ) and 40  $\mu\text{L}$   $\text{NaB}(\text{C}_2\text{H}_5)_4$  were added into 40 mL brown glass bottles, then fully mixed and reacted for 2 h. The recovery rates in water samples ( $n = 7$ ) were analyzed by the certified solution addition, ranging from 81.62% to 86.70%. The standard solution of MeHg (GBW08675) was certified by National Institute of Metrology, with the  $76.30 \pm 2.90 \mu\text{g/g}$  MeHg in the matrix of methanol. The CVs varied from 7.96% to 14.08%. The DL of MeHg in water samples was 0.05 ng/L.

0.1 g solid samples, 5 mL 18% (m/V)  $\text{KBr/H}_2\text{SO}_4$ , 1 mL 1 M  $\text{CuSO}_4$  and 10 mL  $\text{CH}_2\text{Cl}_2$  were sequentially taken into the 40 mL brown glass bottles, fully mixed for 2 h, then centrifuged for 20 min at 3000 r/min. Then 50 mL deionized water was added on collected organic phase for back extraction at  $55 \sim 65^\circ\text{C}$ . After that, 1 mL extracted solution, 30 mL pH buffer ( $\text{pH} = 4.6$ ), 40  $\mu\text{L}$  derivatization reagent and deionized water were taken into 40 mL brown glass bottles, then fully mixed and reacted for 2 h for MeHg analysis. The recovery rates of MeHg in certified material ranged from 80.76%  $\sim$  91.32%. The standard material of Methylmercury and Elements in Lake Sediment (GBW08308) were certified by National Institute of Metrology, with the concentration of  $5.20 \pm 0.70 \text{ ng/g}$  MeHg in lake sediments. The tested CVs were less than 15% (7.10%  $\sim$  14.36%). The DL of MeHg in solid samples was 0.04  $\mu\text{g/kg}$ .

Extracted Hg fractions in solid samples were analyzed by the modified Tessier procedure. The detailed extracted procedures of Hg fractions in solid samples are provided in Table S1.

### 2.3.3. Hg isotope analyses

Hg isotope values were analyzed using a multi-collector inductively coupled plasma mass spectrometer (MC-ICP-MS) at Chinese Academy of Sciences. Briefly, 0.5 g soil samples, 5 mL aqua regia and 0.2 mL  $\text{BrCl}$  were added in glass vessel to fully digest ( $95^\circ\text{C}$ , 12 h). After digestion, 0.5 mL  $\text{NH}_2\text{OH}\cdot\text{HCl}$  was added subsequently to fully degrade residual  $\text{BrCl}$ . After centrifugation, the collected supernatants were adjusted to 0.5  $\mu\text{g/L}$  THg and within 20% acidity. In Hg isotope analysis process, the instrumental parameters are detailed in Table S2. The Hg isotope values were referred to the bracketed standard Hg (NIST 3133), and MDF is expressed by  $\delta^{202}\text{Hg}$ :

$$\delta^{\text{xxx}}\text{Hg}(\text{‰}) = \left\{ \left( \frac{\text{xxxHg}/^{198}\text{Hg}}{\text{sample}} \right) / \left( \frac{\text{xxxHg}/^{198}\text{Hg}}{\text{NIST3133}} \right)^{-1} \right\} \times 1000 \quad (1)$$

The MIF is expressed by  $\Delta^{199}\text{Hg}$ ,  $\Delta^{200}\text{Hg}$  and  $\Delta^{201}\text{Hg}$  and calculated as:

$$\Delta^{199}\text{Hg} \approx \delta^{199}\text{Hg} - (\delta^{202}\text{Hg} \times 0.2520) \quad (2)$$

$$\Delta^{200}\text{Hg} \approx \delta^{200}\text{Hg} - (\delta^{202}\text{Hg} \times 0.5024) \quad (3)$$

$$\Delta^{201}\text{Hg} \approx \delta^{201}\text{Hg} - (\delta^{202}\text{Hg} \times 0.7520) \quad (4)$$

The analytic uncertainties were determined by the largest 2 SD among standard materials (NIST 3177 ( $n = 4$ ) and GSS-5 ( $n = 2$ )) (i.e., 0.07‰, 0.03‰, 0.04‰ and 0.05‰ for  $\delta^{202}\text{Hg}$ ,  $\Delta^{199}\text{Hg}$ ,  $\Delta^{200}\text{Hg}$  and  $\Delta^{201}\text{Hg}$  values, respectively), and the data are detailed in Table S3.

### 2.3.4. Physicochemical analysis

The analysis methods of the physicochemical characteristics in various environmental media are detailed in Text S2.

## 2.4. Allocation, enrichment, transfer and atmospheric deposition

The distribution coefficient ( $K_d$ , L/kg) was used to explore the Hg partitioning behaviors in aquatic ecosystems. The enrichment factor (EF) was used to assess the enrichment degrees of Hg in solid samples. The bioaccumulation factor (BAF) and bioconcentration factor (BCF) were

adopted to evaluate the enrichment ability of Hg in the aboveground parts and underground parts in vegetables, respectively. The calculation formula, parameters and evaluation criteria are presented in Text S3.

The atmospheric Hg deposition fluxes were calculated by Eq. (5):

$$D_{\text{Hg}} = \frac{C_{\text{Hg}} \times m}{S} \quad (5)$$

where  $D_{\text{Hg}}$  is the mass of deposited Hg ( $\text{mg/m}^2/\text{y}$ );  $C_{\text{Hg}}$  refers to the Hg concentrations in dust falls ( $\text{mg/kg}$ );  $m$  refers the deposited mass in a container ( $\text{kg/y}$ );  $S$  represents the area of a container ( $\text{m}^2$ ).

Based on the current deposition fluxes, the annual contributions of atmospheric Hg deposition on surface soils were estimated [22] as following Eq. (6):

$$F_{\text{Hg}} = \frac{D_{\text{Hg}}}{\rho_{\text{soil}} \times z} \quad (6)$$

Where  $F_{\text{Hg}}$  is the contribution of atmospheric Hg deposition on surface soils ( $\text{mg/kg/y}$ ),  $\rho$  represents the soil density ( $1125 \text{ kg/m}^3$ );  $z$  indicates the topsoil thickness (0.2 m) [22,5].

The temporal changes of Hg in surface soils under the present Hg deposition fluxes could be evaluated by the following recursion formula and detailed in Text S4:

$$C_n^{\text{Hg}} = C_0^{\text{Hg}} + F_{\text{Hg}}R \frac{1 - R^n}{1 - R} \quad (7)$$

where  $C_n^{\text{Hg}}$  represents the predicted Hg concentrations in surface soils after  $n$  years ( $\text{mg/kg}$ );  $C_0^{\text{Hg}}$  indicates the detected Hg concentrations in currently collected surface soils ( $\text{mg/kg}$ );  $R$  is the retention rate of Hg in soils (%).

## 2.5. Quantifying of Hg sources in surface soils

The relative contributions of atmospheric Hg deposition to surface soils were quantified by a binary model [34], as follows:

$$X\delta^{202}\text{Hg}_{\text{atm}} + Y\delta^{202}\text{Hg}_{\text{bac}} = \delta^{202}\text{Hg}_{\text{soils}} \quad (8)$$

$$X + Y = 1 \quad (9)$$

where  $X$  and  $Y$  were the relative contributions in the surface soils of atmospheric deposition and background source, respectively.

## 2.6. Environmental risk assessment

### 2.6.1. Ecological risk assessment

Ecological risk (ER) of total content index and risk assessment code (RAC) of mobile fractions index were used to evaluate static risk in sediments and soils and are provided in Text S5.

The DGH model developed by Zheng et al. [53] revealed the transformation paths from stable Hg fractions to active Hg fractions in soils, and has been widely applied in the dynamic risk assessment in Hg contaminated sites [3]. The model fitted nonlinear pathways from “total releasable content of pollutant (TRCP)” to “total content of active species (TCAS)”. The curve equation was as follows:

$$Q = a_0 + a_1C + a_2C^2 + a_3C^3 + \dots \quad (10)$$

The critical indicators and characteristics of the equation are listed in Text S6. The burst probability of DGH ( $P_{\text{DGH}}$ ) could be accurately predicted by Eq. (11):

$$P_{\text{DGH}} = \text{Sample}_{\text{exceedance}} / \text{Sample}_{\text{total}} \quad (11)$$

where  $\text{Sample}_{\text{exceedance}}$  indicated the sample numbers with TRCP value exceeding burst critical point (BCP) value in sediments and soils, and  $\text{Sample}_{\text{total}}$  indicated the total sample numbers in sediments and soils.

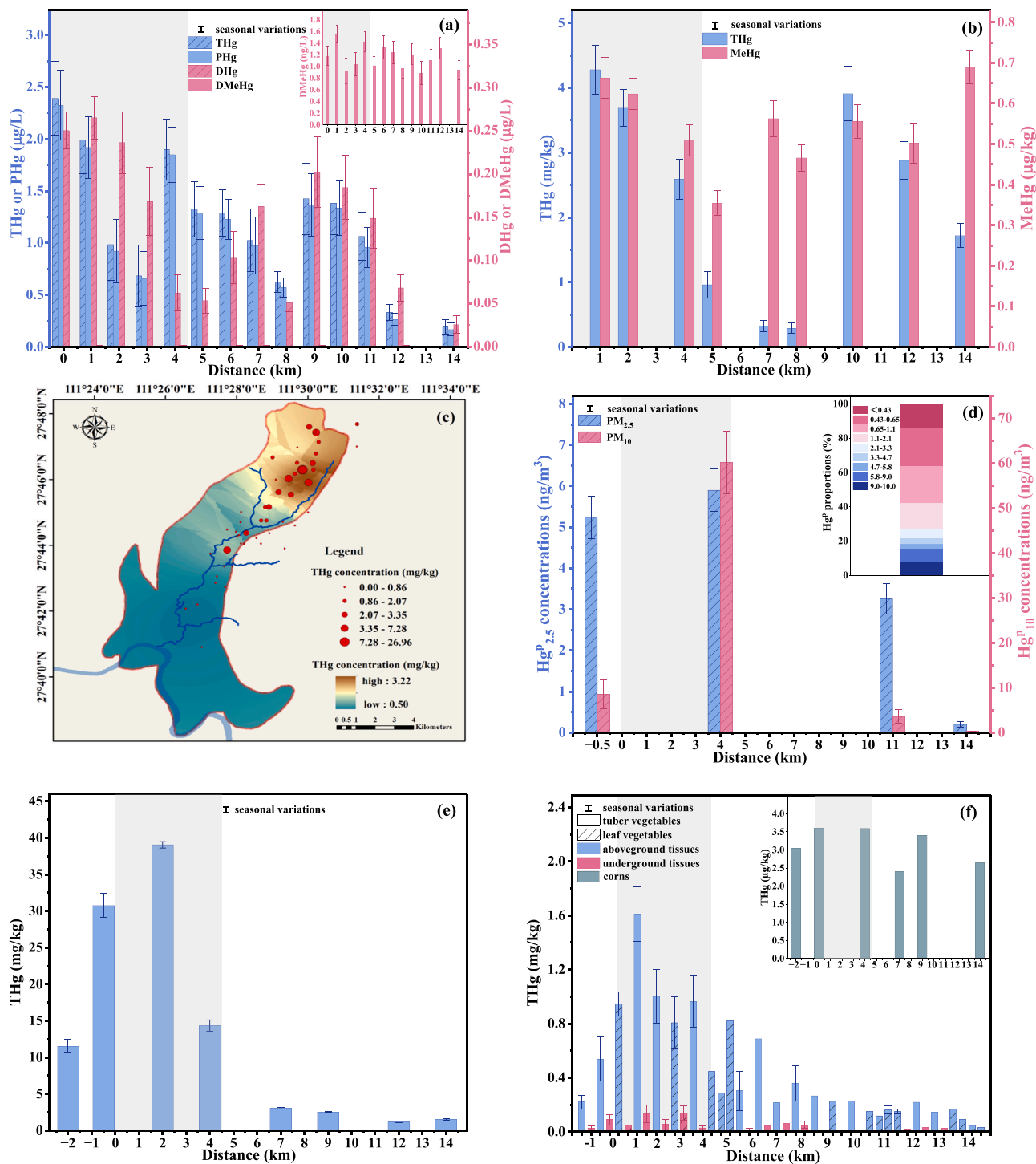


Fig. 2. The Hg contents in river water (a), sediments (b), soils (c), atmospheric particulate matters (d), dust falls (e) and crops (f) in the study area (The error bars represented seasonal variations; the shaded zones represented the XKS area).

2.6.2. Human health risk assessment

Local residents faced the potential Hg risks from multiple pathways, including soils, atmospheric particulate matters, vegetables and corns. As the result of unclear carcinogenic effect of Hg, this study only evaluated the non-carcinogenic risks of Hg. The hazard index (HI), the ratio of chronic daily intake (CDI) to reference dose (RfD), was often adopted to assess the non-carcinogenic risks of THg and MeHg [52].

The CDI value of water by oral ingestion and dermal contact were calculated by Eq. (12), (13):

$$CDI_{ow} = \frac{C_{ow} \times IR_w \times ABS_g \times EF_w \times ED_w}{BW \times AT_w} \tag{12}$$

$$CDI_{dw} = \frac{C_{dw} \times SA \times K_p \times EF_w \times ED_w \times ET}{BW \times AT_w} \tag{13}$$

The CDI values of soils by oral ingestion and dermal contact were calculated by Eq. (14), (15):

$$CDI_{oso} = \frac{C_{so} \times IR_{so} \times EF_{so} \times ED_{so}}{BW \times AT_{so}} \times 10^{-6} \tag{14}$$

$$CDI_{dso} = \frac{C_{so} \times ABS \times EF_{so} \times ED_{so} \times SA \times AF}{BW \times AT_{so}} \times 10^{-6} \quad (15)$$

The CDI values of particulate-bound Hg (PM<sub>10</sub>) in atmosphere were quantified by inhalation, and calculated by Eq. (16):

$$CDI_{par} = \frac{C_{par} \times DAIR \times ED_{par} \times PIAF \times (f_{s_{po}} \times EFO + f_{s_{pi}} \times EFI)}{BW \times AT} \times 10^{-3} \quad (16)$$

The CDI values of Hg in vegetables and corns by oral ingestion were determined by Eq. (17), (18), respectively:

$$CDI_{oveg} = \frac{(C_{leaf} \times IR_{leaf} + C_{tuber} \times IR_{tuber}) \times EF_{veg} \times ED_{veg} \times CF_{veg}}{BW \times AT_{veg}} \times 10^{-3} \quad (17)$$

$$CDI_{ocorn} = \frac{C_{corns} \times IR_{corns} \times EF_{corns} \times ED_{corns} \times CF_{corns}}{BW \times AT_{corns}} \times 10^{-3} \quad (18)$$

The HI values were calculated by the following Eq. (19):

$$HI = \sum THQ_i = \sum \frac{CDI_i}{RfD_i} \quad (19)$$

The mathematical meaning and referenced values of critical indicators for Hg exposure by multiple pathways are provided in Table S4. The calculated HI values were compared with the threshold (1) set by USEPA to determine whether multi-path exposure posed Hg risks to human health. A HI value > 1 represents Hg exposure by these pathways would pose adverse health impact on local residents. Conversely, it would be considered that no health risk was caused on local residents.

### 3. Results and discussion

#### 3.1. Hg contamination in environment

The detected characteristics of environmental samples in river water, sediments and soils are showed in Text S7 and Table S5. The Hg contents of various environmental media in varied seasons are presented in Table S6.

##### 3.1.1. Hg contents in river water

In river water, the THg concentrations varied from 0.19 µg/L to 2.39 µg/L (average: 1.16 ± 0.63 µg/L). The extremely high THg concentration (2.39 µg/L) was found nearby smelters in North Mine, which was lower than the Chinese emissions standards of industries wastewater (5 µg/L) (GB 30770–2014). The THg contents in the Lianxi River were comparable with those in river near Wanshan Hg mine in China (0.004 ~ 3.20 µg/L) [21] and in river surrounding Xiushan Hg mine in China (0.02 ~ 2.39 µg/L) [45]. The THg contents in the Lianxi River were higher than those in the Shuichang River (0.08 ~ 0.40 µg/L) [7], which was not directly polluted by antimony mine drainage.

In Fig. 2a, the concentrations of THg, DHg and PHg decreased with the river transportation. Affected by coal mining plant located 8.5 km downstream of the North Mine, the rapid increase of THg, DHg and PHg contents in LX-12 were observed. These Hg contents at the confluence of the Lianxi River and Zijiang River (14 km downstream of the North Mine and 5.5 km downstream of the coal mining plant), reduced to 0.19 µg/L, 0.17 µg/L and 0.03 µg/L, respectively, which met the Class IV (1 µg/L) of Quality Standard for Surface Water in China (GB3838–2002). Except the dilution effect, the settlement of particles during river transportation was probably a crucial explanation for the reduction of Hg contents in river water. PHg was the dominant speciation of THg (87.74 ± 4.06%), which might attribute that most Hg in the Lianxi River was mainly related to particles. The DMeHg concentrations varied from 0.89 to 1.56 ng/L (1.15 ± 0.21 ng/L). No obvious trend of MeHg distribution was shown with river transportation.

The THg and PHg contents in summer were significantly higher than those in spring and autumn ( $p < 0.01$ ) in river water (Table S6). It was mainly attributed to frequent rainfall in summer, which led to large amounts of Hg-containing leachate and wastewater discharged from mining and smelting activities being flowed into the river through surface runoff. No significant seasonal variations were observed in DHg and DMeHg contents.

##### 3.1.2. Hg contents in sediments

In sediments, the THg concentrations largely ranged from 0.30 mg/kg to 4.28 mg/kg (average: 2.01 ± 1.64 mg/kg), which exceeded the probable effect value (1.06 mg/kg) of Sediment Quality Guidelines (SQG). The THg contents in sediments in the Lianxi River were higher than those reported THg contents in Shileixi Creek surrounding Xiushan manganese mine in China (0.19 ~ 1.23 mg/kg, 0.63 ± 0.27 mg/kg) [51] and Gambia River around the gold mine in Senegal (0.02 ~ 2.40 mg/kg, 1.16 ± 0.80 mg/kg) [27]. Although industrial discharges of coal mining caused rapid increase of THg content at 8.5 km downstream of the North Mine, THg contents in sediments considerably decreased with the distance from the pollution source during river transportation (Fig. 2b). In addition, no significant seasonal variations of THg contents in sediments were observed ( $p > 0.05$ ) (Table S6).

The proportions of extracted Hg fractions in sediments are provided in Fig. S2. Obviously, Hg in sediments mainly existed in the form of residual components (83.14 ± 4.63%) and organic bound components (15.17 ± 4.04%). The MeHg concentrations were from 0.35 µg/kg to 0.69 µg/kg (average: 0.54 ± 0.11 µg/kg). MeHg contents in sediments showed no significant distribution trend and seasonal variations ( $p > 0.05$ ).

##### 3.1.3. Hg contents in soils

In soils, the THg contents considerably varied from 0.13 mg/kg to 26.96 mg/kg (average: 1.87 ± 3.88 mg/kg). 29.41% samples exceeded the risk screening values for soil contamination of agricultural land and 7.84% samples exceeded the risk intervention values for soil contamination of agricultural land (GB15618–2018). The THg concentrations in soils in the study area were lower than THg concentrations reported in soils surrounding Hg mine in the Xiushan region of Chongqing (0.45 ~ 68 mg/kg, 9.80 ± 17.50 mg/kg) [45] and higher than the THg concentrations in a Pb/Zn smelter area in Hunan (0.86 ~ 1.50 mg/kg, 1.07 ± 0.22 mg/kg) [19]. The THg contents in soils in the XKS were significantly higher than those outside the XKS ( $p < 0.01$ ), and the THg contents in the XKS showed a decreasing trend from the North Mine to South Mine. The THg contents in soils displayed no significant seasonal variations ( $p > 0.05$ ) (Table S6).

The dominant species in soils were residual Hg (87.72 ± 7.73%) and organic bound Hg (10.93 ± 7.63%) (Fig. S2). The MeHg contents in soils varied from 0.28 µg/kg to 1.33 µg/kg (average: 0.55 ± 0.21 µg/kg). No obvious distribution pattern (Fig. S3) and seasonal variations of MeHg in soils were observed ( $p > 0.05$ ).

##### 3.1.4. Hg contents in atmospheric particulate matters

In the study area, the daily average concentrations of PM<sub>2.5</sub> and PM<sub>10</sub> were 29.16 ± 13.09 µg/m<sup>3</sup> and 56.72 ± 40.12 µg/m<sup>3</sup>, respectively, which met the Class II (35 µg/m<sup>3</sup> and 70 µg/m<sup>3</sup> for PM<sub>2.5</sub> and PM<sub>10</sub>, respectively) of Ambient Air Quality Standard in China (GB 3095–2012). The daily average Hg concentrations in PM<sub>2.5</sub> (Hg<sub>2.5</sub><sup>p</sup>) and PM<sub>10</sub> (Hg<sub>10</sub><sup>p</sup>) in the study area were 1.17 ± 1.93 ng/m<sup>3</sup> and 7.87 ± 18.68 ng/m<sup>3</sup>, respectively. In Fig. 2d, the highest concentrations of Hg<sub>2.5</sub><sup>p</sup> and Hg<sub>10</sub><sup>p</sup> were observed in the XKS (5.90 ng/m<sup>3</sup> and 60.06 ng/m<sup>3</sup>, respectively), and obviously decreased away from the XKS. In the Lengshuijiang City, 14 km away from the XKS, the concentrations of Hg<sub>2.5</sub><sup>p</sup> and Hg<sub>10</sub><sup>p</sup> were 0.03 ng/m<sup>3</sup> and 0.06 ng/m<sup>3</sup>, respectively. The contents of Hg<sub>2.5</sub><sup>p</sup> and Hg<sub>10</sub><sup>p</sup> in the study area were higher than those in a power plant in Southwest China (0.14 ng/m<sup>3</sup> and 0.19 ng/m<sup>3</sup>, respectively) [50]. The Hg<sub>2.5</sub><sup>p</sup> contents in the Lengshuijiang City were lower

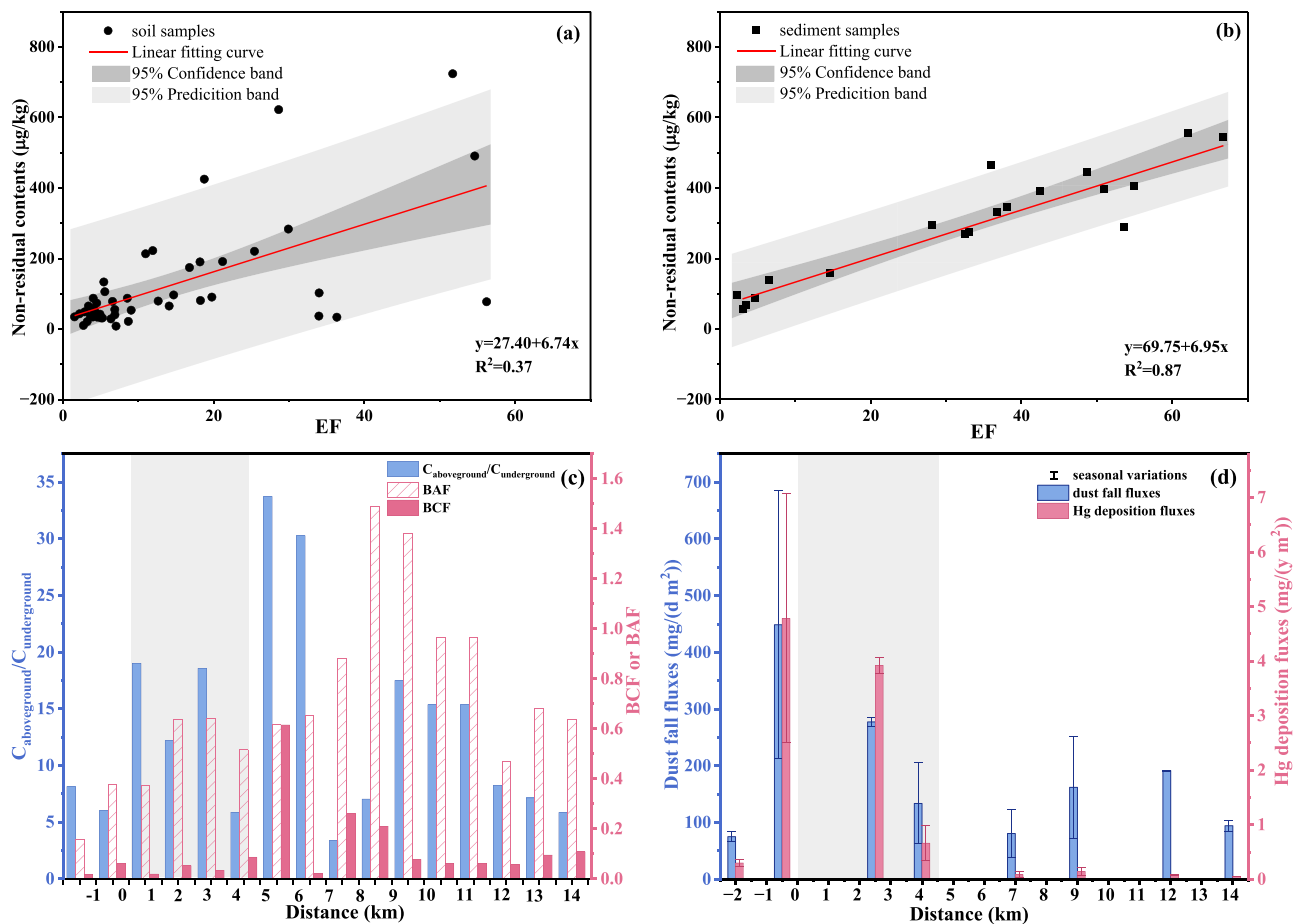


**Fig. 3.** The Hg enrichment degree in soils (a) and sediments (b), the translocation factors in vegetables (c) and dust fall fluxes and annual Hg deposition fluxes (d) in sampling sites in the study area.

than those in Guiyang City ( $0.10 \text{ ng/m}^3$ ) [20] and the  $\text{Hg}_{10}^0$  contents in the Lengshuijiang City were comparable with those in Xiamen City ( $0.06 \text{ ng/m}^3$ ) [36]. The average proportion of  $\text{Hg}_{2.5}^0$  to  $\text{Hg}_{10}^0$  was  $59.95 \pm 24.51\%$ , indicating the particulate-bound Hg in  $\text{PM}_{10}$  mainly existed in fine particles, which was proved by distribution of PHg in particles with different sizes (Fig. 2d). Based on the investigation, the intensity of industrial activities in the XKS were not affected by varied seasons. Moreover, local residents didn't use coal burning for indoor heating. In addition, the sampling time in summer was in the Plum Rainy Season, with high rainfall. The contents of  $\text{Hg}_{2.5}^0$  and  $\text{Hg}_{10}^0$  in spring were significantly higher than those in summer ( $p < 0.01$ ) (Table S6), which was attributed to the removal of atmospheric particulate matters by frequent rainfall in summer.

The Hg concentrations in dust falls ranged from  $1.20 \text{ mg/kg}$  to  $39.05 \text{ mg/kg}$ , with an average of  $13.01 \pm 14.53 \text{ mg/kg}$ , which was lower than those in Wanshan Hg mine ( $1 \sim 39.12 \text{ mg/kg}$ ,  $30.59 \text{ mg/kg}$ ) and higher than those in Xunyang Hg mine ( $2.99 \sim 14.01 \text{ mg/kg}$ ,  $3.50 \text{ mg/kg}$ ) (Sun et al., 2020). The THg concentrations of dust falls in the XKS ( $23.93 \pm 13.18 \text{ mg/kg}$ ) were significantly higher than those outside the XKS ( $2.08 \pm 0.86 \text{ mg/kg}$ ) ( $p < 0.01$ ). The THg contents in dust falls were significantly higher (3.73 ~ 22.71 times) than those in soils at the corresponding locations ( $p < 0.01$ ). The THg contents in dust falls presented no significant difference in varied seasons ( $p > 0.05$ ) (Table S6).

### 3.1.5. Hg contents in crops

In Fig. 2f, the THg contents in vegetables in the XKS ( $0.52 \pm 0.48 \text{ mg/kg}$ ) were higher than those outside the XKS ( $0.21 \pm 0.17 \text{ mg/kg}$ ), and showed a decreasing trend from North Mine to

South Mine. The THg contents of vegetables in the XKS were lower than those in the Wanshan Hg mining region ( $1.70 \pm 1.90 \text{ mg/kg}$ ) [30] and higher than those in the Shenda gold mine ( $0.14 \pm 0.09 \text{ mg/kg}$ ) [32]. In Fig. 2f, the THg contents of vegetables in aboveground tissues ( $0.53 \pm 0.44 \text{ mg/kg}$ ) were significantly higher than those in underground tissues ( $0.05 \pm 0.04 \text{ mg/kg}$ ) ( $p < 0.01$ ). THg contents of edible tissues in leaf vegetables were significantly higher than those in tuber vegetables and crops in the corresponding sites ( $p < 0.01$ ). The THg contents of vegetables in summer were significantly higher than those in autumn ( $p < 0.01$ ) (Table S6), which might be affected by collected vegetable species. In addition, no significant differences of THg concentrations in corns were observed in the XKS ( $3.16 \pm 1.57 \text{ µg/kg}$ ) and outside the XKS ( $3.02 \pm 0.54 \text{ µg/kg}$ ) ( $p > 0.05$ ). The THg contents in vegetables in the study area all exceeded the limit of THg in vegetables (Hg:  $0.01 \text{ mg/kg}$ ), whereas the THg contents in corns were all below the limit value (Hg:  $0.02 \text{ mg/kg}$ ) (GB2762–2012).

The MeHg in collected vegetables and corns ranged from  $0.10 \text{ µg/kg}$  to  $0.39 \text{ µg/kg}$  (average:  $0.24 \pm 0.10 \text{ µg/kg}$ ). No significant variations of MeHg contents in crops were observed in different regions and seasons ( $p > 0.05$ ). In addition, the MeHg contents in aboveground tissues ( $0.21 \pm 0.12 \text{ µg/kg}$ ) were lower than those in underground tissues ( $0.29 \pm 0.18 \text{ µg/kg}$ ).

## 3.2. Environmental behaviors of Hg

### 3.2.1. Allocation, enrichment and transfer of Hg

In the Lianxi River, the average  $\log K_d$  values of THg were  $4.36 \pm 0.57$  and  $4.24 \pm 0.63$  in the XKS area and outside the XKS area, respectively, which were comparable with the reported  $\log K_d$  of THg in

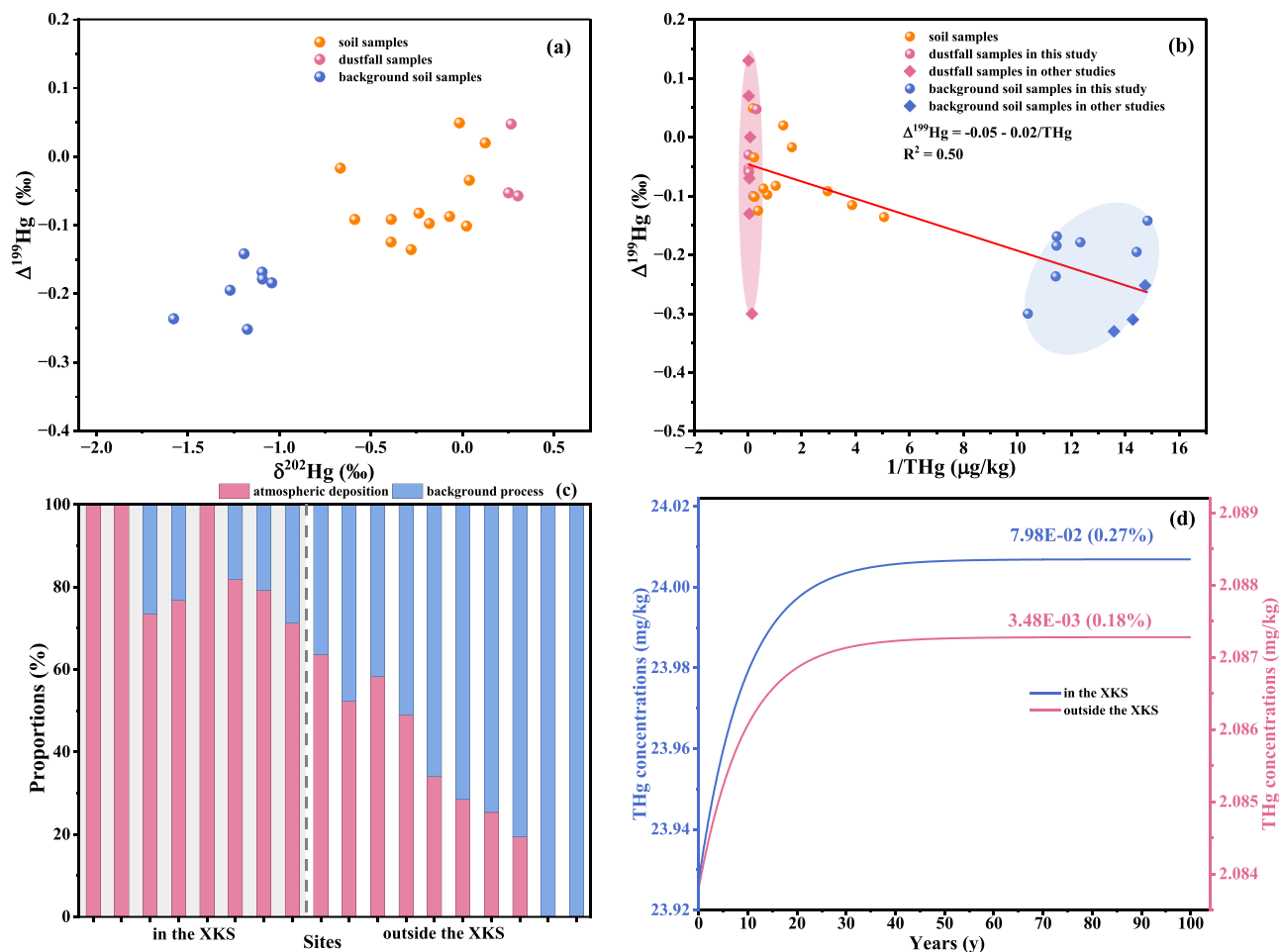


Fig. 4. Hg isotope compositions of contaminated surface soils, dust falls and regional background soils (a), plot of  $\Delta^{199}\text{Hg}$  and  $1/\text{THg}$  in above environmental samples (b), relative contributions of two Hg sources in surface soils (c) and temporal changes of Hg in surface soils under the atmospheric deposition (d).

16 river mouths in China ( $4.30 \pm 0.39$ ) [23,49]. The average  $\log K_d$  values of MeHg were  $2.67 \pm 0.18$  and  $2.81 \pm 0.08$  in the above regions, respectively. No significant differences in allocation coefficients of THg and MeHg were observed in the XKS and outside the XKS in the Lianxi River.

Hg in sediments and soils were strongly enriched ( $30.58 \pm 24.71$ ) and significantly enriched ( $16.26 \pm 18.42$ ), respectively. In comparison, the Hg in sediments and soils in the XKS ( $31.69 \pm 33.34$  and  $16.15 \pm 4.79$ , respectively) presented higher enrichment than those outside the XKS ( $29.11 \pm 12.58$  and  $13.73 \pm 1.53$ , respectively). The Hg enrichment degree in sediments in the Lianxi River was comparable with that in sediments in the Břilina River affected by coal mining (strong enrichment) [38]. The Hg enrichment degree in soils in this antimony-coal mine area was higher than that in soils surrounding the mines and quarries (moderate enrichment) in Yunan (Liu et al., 2023) and lower than that in forest soils around a cement plant in Europe (strong enrichment) [2]. The significant correlations between non-residual components and EF values in samples ( $p < 0.05$ ) proved that soils in the XKS (Fig. 3a) and sediments in the Lianxi River (Fig. 3b) were greatly impacted by anthropogenic activities [12].

As shown in Fig. 3c, the differences of BAF and BCF values were not significant with different distances from the North Mine. The BCF values and BAF values of vegetables in the XKS were  $0.12 \pm 0.15$  and  $0.72 \pm 0.35$ , respectively. The BAF values were higher than BCF values, indicating the aboveground tissues accumulated more Hg than the underground tissues. The THg contents in aboveground tissues were  $13.37 \pm 8.88$  times (3.39 ~ 33.72 times) higher than those in underground tissues in the study area, which was significantly higher than the

reported values caused by root uptake (0 ~ 2 times) [28]. Shahid et al. [33] reported the foliar accumulation of heavy metal from atmospheric deposition greatly enhanced contamination in aboveground tissues in plants near smelters. Therefore, high Hg contents of aboveground tissues in vegetables in this study area might be attributed to the foliar accumulation caused by atmospheric deposition from smelters.

### 3.2.2. Atmospheric deposition of Hg

The dust falls fluxes in the XKS ( $83.46 \sim 615.66$ ,  $286.77 \pm 179.03 \text{ mg/m}^2/\text{d}$ ) were higher than outside the XKS ( $50.69 \sim 226.05$ ,  $120.92 \pm 59.91 \text{ mg/m}^2/\text{d}$ ). The dust falls fluxes in the XKS were higher than recommended value in Ambient Air Quality Standard of Dust Falls in some provinces in China ( $200 \text{ mg/m}^2/\text{d}$ ) (DB52/1699-2022). The annual Hg deposition fluxes in the XKS ( $0.44 \sim 6.40$ ,  $3.12 \pm 2.20 \text{ mg/m}^2/\text{d}$ ) were significantly higher than those outside the XKS ( $0.05 \sim 0.34$ ,  $0.13 \pm 0.10 \text{ mg/m}^2/\text{d}$ ) ( $p < 0.01$ ), which might be caused by the increased particle fluxes and Hg contents in atmosphere from intensive anthropogenic activities in the mining area (3.1.4 section) (Fig. 3d). The annual atmospheric Hg deposition fluxes in the XKS were higher than those in zinc refinery in European (maximum deposition:  $0.99 \text{ mg/m}^2/\text{d}$ ) [35] and lower than those in a historical Hg mine in Tongren ( $6.77 \text{ mg/m}^2/\text{d}$ ) [22]. Furthermore, annual input of atmospheric Hg deposition in surface soils in the XKS ( $13.89 \pm 9.79 \text{ } \mu\text{g/kg}$ ) was higher than those outside the XKS ( $0.59 \pm 0.45 \text{ } \mu\text{g/kg}$ ).

### 3.2.3. Impact of atmospheric Hg deposition on surface soils

Some studies reported that atmospheric deposition is the primary heavy metal source in surface soils in highly developed industry areas

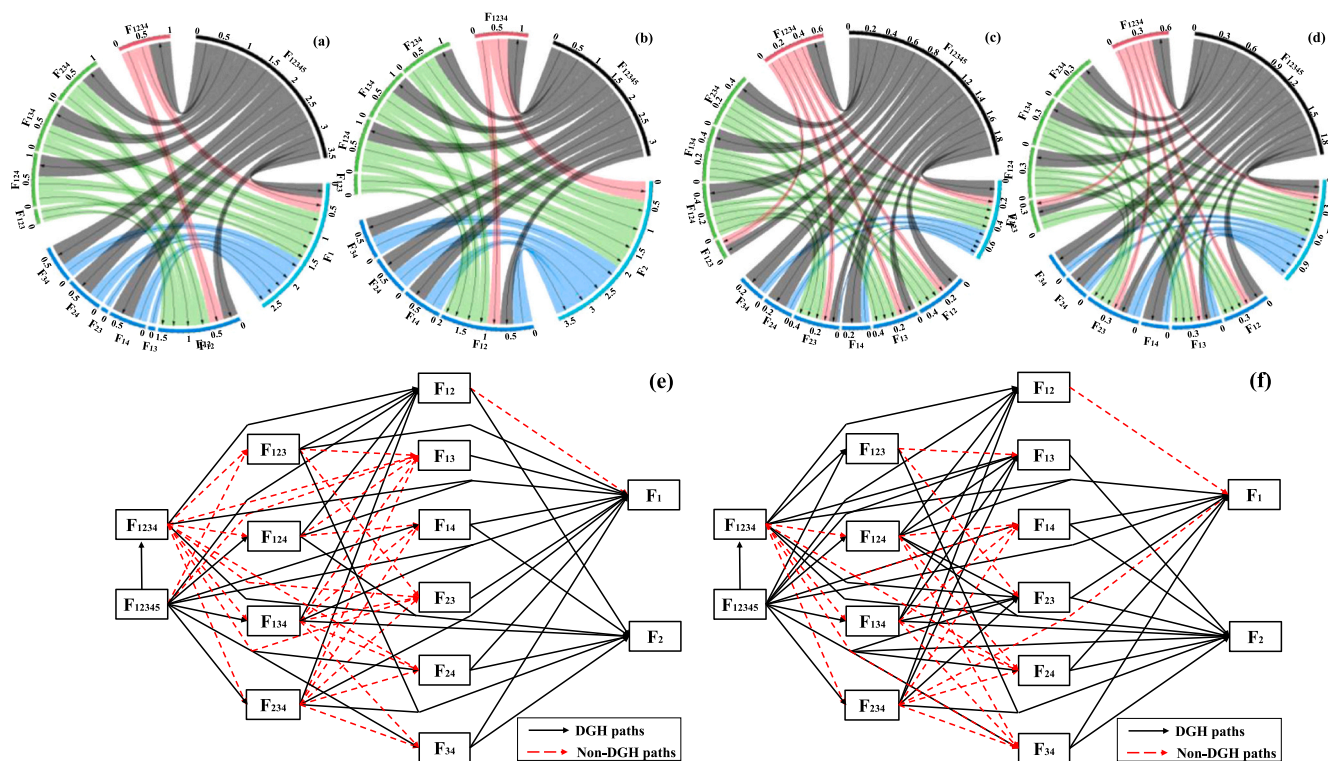


**Fig. 5.** The DGH pathways of Hg in sediments (ending with  $F_1$  (a) and ending with  $F_2$  (b)) and soils (ending with  $F_1$  (c) and ending with  $F_2$  (d)), and all transformation pathways of Hg from TRCP to TCAS in sediments (e) and soils (f). The arrow direction is the transformation pathways.

([34,5]; Liu et al., 2023). In this study, the impact of atmospheric Hg deposition on surface soils was analyzed by Hg isotope signatures in dust falls and surface soils. The  $\delta^{202}\text{Hg}$  and  $\Delta^{199}\text{Hg}$  values of dust falls in the XKS ranged from 0.25‰ to 0.30‰ ( $0.27 \pm 0.03\%$ ) and  $-0.06\%$  to 0.05‰ ( $-0.02 \pm 0.06\%$ ), respectively. The  $\delta^{202}\text{Hg}$  and  $\Delta^{199}\text{Hg}$  values of contaminated soils in the XKS varied from  $-0.92\%$  to 0.12‰ ( $-0.26 \pm 0.32\%$ ) and  $-0.14\%$  to 0.05‰ ( $-0.07 \pm 0.06\%$ ), respectively. The  $\delta^{202}\text{Hg}$  and  $\Delta^{199}\text{Hg}$  values in background soils with low THg contents from the lower layer profile (below 100 cm) outside the XKS were from  $-1.58\%$  to  $-1.04\%$  ( $-1.20 \pm 0.25\%$ ) and  $-0.24\%$  to  $-0.17\%$  ( $-0.19 \pm 0.03\%$ ), respectively. In general, obviously distinct Hg isotope compositions were observed in dust falls and background soils (Fig. 4a).

Compared with the relationship between  $\Delta^{199}\text{Hg}$  and  $\delta^{202}\text{Hg}$  ( $R^2 = 0.42$ ) (Fig. S4), more significant correlation between  $\Delta^{199}\text{Hg}$  and  $1/\text{THg}$  was showed in samples ( $R^2 = 0.50$ ) ( $p < 0.01$ ). The linear relationship between  $\Delta^{199}\text{Hg}$  and  $1/\text{THg}$  indicated two dominant Hg sources in environmental samples (Fig. 4b). The linear regression met the normality and homogeneity of residuals (Fig. S5). The end-members of  $\Delta^{199}\text{Hg}$  and  $1/\text{THg}$  values for atmospheric deposition source in non-ferrous industrial areas ( $\Delta^{199}\text{Hg}$ :  $-0.05 \pm 0.11\%$ ;  $1/\text{THg}$ :  $0.09 \pm 0.09 \mu\text{g}/\text{kg}$ ,  $n = 12$ ) were estimated by dust falls in a zinc smelter, gold mining area, Hg mining area [34], Sb mining and smelter area (this study) and other non-ferrous metals industrials [17]. The  $\Delta^{199}\text{Hg}$  and  $1/\text{THg}$  values of background source ( $\Delta^{199}\text{Hg}$ :  $-0.23 \pm 0.06\%$ ;  $1/\text{THg}$ :  $13.47 \pm 3.85 \mu\text{g}/\text{kg}$ ,  $n = 10$ ) were determined by uncontaminated soils. The proportions of two Hg sources (atmospheric deposition and background process) in surface soils were quantified by a binary model. Furthermore, atmospheric Hg deposition was the dominant Hg source on surface soils in the XKS (85.34%) and background source had no prominent impact (14.66%) in Hg contamination on surface soils. In addition, background source was the major Hg source on surface soils outside the XKS, atmospheric Hg deposition and background source contributed 33.08% and 66.92% on surface soils, respectively (Fig. 4c). However, the atmospheric deposition in this study only focused on dry

and wet deposition, and the atmospheric deposition pathway of gaseous element Hg carried by litterfall has not been considered.

The recursion model was used to predict the effects of atmospheric Hg deposition on surface soils in the XKS and outside the XKS during the next 100 years. The predicted THg concentrations in soils in all sampling sites increased under the present atmospheric Hg deposition fluxes (Fig. S6). The Hg in surface soils in the XKS and outside the XKS after 100 years increased by 0.27% and 0.18%, respectively (Fig. 4d). The relationship between atmospheric Hg deposition fluxes and Hg concentrations in surface soils provided scientific basis for preventing Hg contamination in soils.

### 3.3. Ecological risk assessment in sediments and soils

#### 3.3.1. Static risk assessment

The ER and RAC values were calculated to assess the static Hg risks in sediments and soils in the study area (Table S7). The ER values in sediments and soils were  $1341.56 \pm 1010.39$  and  $1246.58 \pm 2585.99$ , respectively, showing very high risks of THg in sediments and soils. However, the static risks of THg-orientated assessment might be overestimated, as a result of the stable Hg fractions had low bioavailability and less environment effect [53]. The calculated RAC values based on the mobile fractions in sediments and soils were  $5.52 \pm 2.29$  and  $3.72 \pm 4.26$ , respectively, representing the static Hg risks in solid samples in the study area were low. The higher static Hg risks were observed in sediments and soils in the XKS ( $6.73 \pm 3.04$  and  $5.36 \pm 4.52$ , respectively) than those outside the XKS ( $4.61 \pm 1.32$  and  $3.11 \pm 4.14$ , respectively). Especially near the smelters in North Mine, where the moderate Hg risks in sediments and soils have been found. However, the changed environmental conditions lead to the dynamic variations of Hg risks in sediments and soils.

#### 3.3.2. Dynamic risk assessment

In the processes of dynamic transformation and release, the starting

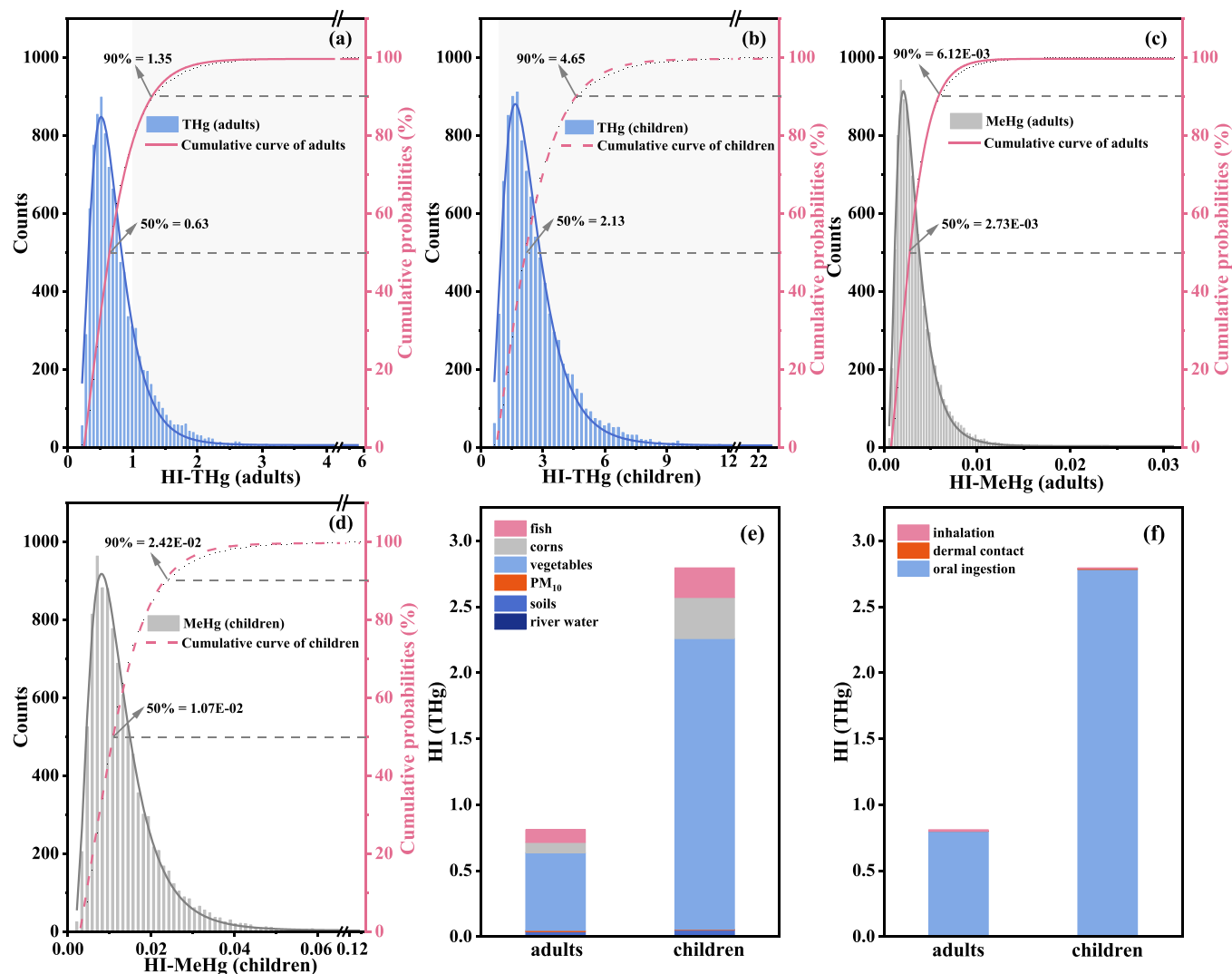


Fig. 6. The probability distributions and HI values caused by THg (a, b) and MeHg (c, d) faced by adults and children in the study area (the grey area indicated the potential health risks), the HI values of THg in various environmental media (e) and HI values of THg caused by multiple pathways (f).

point was set as TRCP and the ending point was set as TCAS. TRCP represented the total of all fractions or some fractions under specific conditions, TCAS represented the single or multiple active fractions. With greater instability and bioavailability potential, exchangeable Hg and carbonate bound Hg were set as the final ending points [3]. The transformation processes from TRCP to TCAS included geochemical paths with different characteristics. Among them, the nonlinear processes were characterized by DGH model, while the linear processes were fitted by linear equations.

In addition to the changes of environmental conditions such as the acidification of sediments and soils caused by mining activities, the continuous input of Hg caused the variations in Hg fractions, which was the key factor inducing nonlinear processes. When the accumulated Hg fractions reached the BCP value, the nonlinear transformation from stable fractions to active fractions was triggered, resulting in the surge of active Hg contents, and then inducing dynamic Hg risks. In Fig. 5 and Table S8, the calculated TRCP values in sediments and soils in the study area ranged from 13.79 to 3130.79  $\mu\text{g}/\text{kg}$  and 3.70 to 3307.17  $\mu\text{g}/\text{kg}$ , respectively. According to the samples with  $\text{TRCP}_{\text{Hg}}$  exceeding BCP, it could accurately predicate that 14.29 ~ 42.86% sediment samples and 8.33 ~ 20.83% soil samples have experienced the dynamic Hg risks. The dynamic Hg risks in the antimony-coal mine area were higher than those in the Hg polluted soils surrounding abandoned pesticide plants in

Hunan (10.5%) [3] and the Hg polluted soils near lead-zinc mining area in southern China (8.3%) [53]. In comparison, more frequent DGH paths and higher probabilities of DGH occurrence were observed in sediments (Table S7), indicating that Hg in sediments has greater dynamic risks in the study area. Furthermore, more Hg fractions in sediments were transformed and released into active Hg fractions, resulting in higher static Hg risks in sediments, which was consistent with the conclusion in 3.3.1. In addition, the sediments and soils in the XKS (14.29 ~ 71.67% and 11.76 ~ 69.23%, respectively) presented higher DGH outbreak probabilities than those outside the XKS (16.67 ~ 66.67% and 0 ~ 23.53%, respectively) (Table S8), implying the solid phases in the polluted areas presented higher dynamic Hg risks.

In addition, the linear process, an important supplement for DGH model, further improved the dynamic transformation pathways. It was reported that when the accumulation of heavy metals in solid phases did not reach the threshold of inducing nonlinear process, the linear transformation process from stable fractions to relatively stable fractions, then to active fractions would realize spontaneously.

#### 3.4. Health risk assessment by multiple-path exposure

According to the Monte Carlo probabilistic prediction, 78.22% adults and 8.01% children were exposed to acceptable Hg risk level ( $\text{HI} = 1$ ) set

by USEPA, indicating some populations in the study area were faced significant THg risk. In Fig. 6a and 6b, the deterministic HI values of THg risks faced by adults and children were 0.81 and 2.80, respectively, which were equal to the 67.28th and 69.07th percentile of the predictive values. The results indicated that 67.28% adults and 69.07% children were exposed to the risk levels below the deterministically estimated HI values. The deterministic HI values in this antimony-coal mine area were lower than those in primary Hg contaminated sites in Shanxi Province (1.56 ~ 131) [52]. Based on the deterministic Hg exposure risks by multiple pathways in environmental media (Fig. 6e and Table S9), health risks of THg for adults from vegetables, fish, corns, soils, river water and PM<sub>10</sub> accounted for 72.64%, 11.88%, 9.67%, 4.34%, 0.15% and 1.31% in the study area, respectively. The deterministic health risks of THg for children from the above pathways were 78.83%, 8.04%, 11.15%, 1.60%, 0.17% and 0.20%, respectively. The higher HI values of THg were found in leaf vegetables (0.58 and 2.16 for adults and children, respectively) than those in tuber vegetables (0.01 and 0.05 for adults and children, respectively) and corns (0.08 and 0.31 for adults and children, respectively). In general, except for leaf vegetables (2.16), the health risks of THg faced by children from other environmental media in the study area were all below the safety threshold. Oral ingestion posed higher health risks of THg than dermal contact and inhalation for adults and children (Fig. 6f). Besides, affected by the high THg pollution in the mining area, the populations in the XKS were faced higher health risks of THg than those outside the XKS (Table S10).

Simultaneously, the probabilistic and deterministic HI values of multiple-paths exposure for MeHg were lower than the threshold, indicating that all populations in the study area faced low health risks caused by MeHg. In Figs. 6c and 6d, the deterministic HI values of MeHg that adults and children faced were 3.60E-03 and 1.42E-02, respectively. Correspondingly, 68.75% adults and 68.94% children were exposed to the risk levels below the deterministically estimated HI values. Oral ingestion posed higher health risk of MeHg than dermal contact for adults and children. In addition, no significant difference was found in HI values of MeHg with different distances from the mining area in the study area ( $p < 0.05$ ) (Table S10).

#### 4. Conclusion

The contamination, environmental behaviors and risks of Hg in various environmental media were comprehensively investigated in a typical antimony-coal mining area. The THg contents in river water, sediments, soils, atmospheric particulate matters, vegetables and corns were significantly affected by non-ferrous metals and coal industries, and decreased away from industrial activities. Foliar accumulation caused by atmospheric deposition from smelters contributed to high THg contents of aboveground tissues in vegetables. The binary model based on isotope signatures of dust falls and surface soils verified atmospheric deposition greatly affected Hg contamination on surface soils in the XKS. However, the atmospheric deposition pathway of gaseous element Hg carried by litterfall has not been considered in this study. Compared with soils, the sediments presented more frequent DGH paths and higher burst probabilities of dynamic Hg risks, indicating more Hg fractions were transformed to exchangeable Hg and carbonate bound Hg, further caused greater static Hg risks. Children faced higher Hg risk of multiple exposure than adults. In addition, oral ingestion was the most noteworthy route for Hg exposure, especially for consuming leaf vegetables. Continuous long-term monitoring is crucial for protecting the eco-environment and local residents.

#### Environmental implication

With high toxicity and bioavailability, mercury (Hg) has been regarded as a top ten hazardous chemical by World Health Organization. Human activities promoted Hg enrichment in environment. Emitted Hg from non-ferrous metals mining and smelting constitutes vital

proportions (15%) of anthropogenic Hg emissions. Xikuangshan (XKS) containing resources of non-ferrous metals and coal has been mined more than 120 years. This study comprehensively investigated contamination, environmental behaviors and risks of Hg in various environmental media in the XKS. Relative contributions of atmospheric Hg deposition on soils were quantified in atmosphere-soil system, which provided scientific basis for preventing Hg contamination in soils.

#### Declaration of Competing Interest

The authors declare that they have no known competing financial interests or personal relationships that could have appeared to influence the work reported in this paper.

#### Data Availability

Data will be made available on request.

#### Acknowledgements

This study was supported by the National Key Research and Development Program (Project No. 2023YFC3709101) and the National Natural Science Foundation of China (Project No. 42030706).

#### Appendix A. Supporting information

Supplementary data associated with this article can be found in the online version at doi:10.1016/j.jhazmat.2024.133880.

#### References

- [1] Bavec, S., Biester, H., Gosar, M., 2018. A risk assessment of human exposure to mercury-contaminated soil and household dust in the town of Idrija (Slovenia). *J Geochem Explor* 187, 131–140. <https://doi.org/10.1016/j.jgexplo.2017.05.005>.
- [2] Cutillas-Barreiro, L., Pérez-Rodríguez, P., Gómez-Armesto, A., Fernández-Sanjurjo, M.J., Álvarez-Rodríguez, E., Núñez-Delgado, A., et al., 2016. Lithological and land-use based assessment of heavy metal pollution in soils surrounding a cement plant in SW Europe. *Sci Total Environ* 562, 179–190. <https://doi.org/10.1016/j.scitotenv.2016.03.198>.
- [3] Dong, H.C., Lin, Z.J., Wan, X., Feng, L., 2017. Risk assessment for the mercury polluted site near a pesticide plant in Changsha, Hunan, China. *Chemosphere* 169, 333–341. <https://doi.org/10.1016/j.chemosphere.2016.11.084>.
- [4] Fan, D.L., Zhang, T., Ye, J., 2004. The Xikuangshan Sb deposit hosted by the Upper Devonian black shale series, Hunan, China. *Ore Geol Rev* 24 (1–2), 121–133. <https://doi.org/10.1016/j.oregeorev.2003.08.005>.
- [5] Feng, W.L., Guo, Z.H., Peng, C., Xiao, X.Y., Shi, L., Zeng, P., et al., 2019. Atmospheric bulk deposition of heavy metal(oids) in central south China: fluxes, influencing factors and implication for paddy soils. *J Hazard Mater* 371, 634–642. <https://doi.org/10.1016/j.jhazmat.2019.02.090>.
- [6] Feng, X.B., Foucher, D., Hintelmann, H., Yan, H.Y., He, T.R., Qiu, G.L., 2010. Tracing mercury contamination sources in sediments using mercury isotope compositions. *Environ Sci Technol* 44 (9), 3363–3368. <https://doi.org/10.1021/es9039488>.
- [7] Fu, Z.Y., Wu, F.C., Amarasiriwardena, D., Mo, C.L., Liu, B.J., Zhu, J., et al., 2010. Antimony, arsenic and mercury in the aquatic environment and fish in a large antimony mining area in Hunan, China. *Sci Total Environ* 408 (16), 3403–3410. <https://doi.org/10.1016/j.scitotenv.2010.04.031>.
- [8] Fu, Z.Y., Wu, F.C., Mo, C.L., Deng, Q.J., Meng, W., Giesy, J.P., 2016. Comparison of arsenic and antimony biogeochemical behavior in water, soil and tailings from Xikuangshan, China. *Sci Total Environ* 539, 97–104. <https://doi.org/10.1016/j.scitotenv.2015.08.146>.
- [9] Gao, X., Yuan, W., Chen, J.B., Huang, F., Wang, Z.R., Gong, Y.F., et al., 2023. Tracing the source and transport of Hg during pedogenesis in strongly weathered tropical soil using Hg isotopes. *Geochim Cosmochim Acta* 361, 101–112. <https://doi.org/10.1016/j.gca.2023.10.009>.
- [10] German, C.R., Casciotti, K.A., Dutay, J.C., Heimburger, L.E., Jenkins, W.J., Measures, C.I., et al., 2016. Hydrothermal impacts on trace element and isotope ocean biogeochemistry. *Philos T R Soc A* 374 (2081), 20160035. <https://doi.org/10.1098/rsta.2016.0035>.
- [11] Goix, S., Maurice, L., Laffont, L., Rinaldo, R., Lagane, C., Chmeleff, J., et al., 2019. Quantifying the impacts of artisanal gold mining on a tropical river system using mercury isotopes. *Chemosphere* 219, 684–694. <https://doi.org/10.1016/j.chemosphere.2018.12.036>.
- [12] Gu, X., Ouyang, W., Xu, L., Tysklind, M., Lin, C.Y., He, M.C., et al., 2020. Occurrence, migration, and allocation of arsenic in multiple media of a typical semi-enclosed bay. *J Hazard Mater* 384, 121313. <https://doi.org/10.1016/j.jhazmat.2019.121313>.

- [13] Gu, X., Wang, Z.X., Wang, J., Ouyang, W., Wang, B.D., Xin, M., et al., 2021. Sources, trophodynamics, contamination and risk assessment of toxic metals in a coastal ecosystem by using a receptor model and Monte Carlo simulation. *J Hazard Mater* 424 (B), 127482. <https://doi.org/10.1016/j.jhazmat.2021.127482>.
- [14] Huang, J.L., Wu, Y.Y., Sun, J.X., Li, X., Geng, X.L., Zhao, M.L., et al., 2021. Health risk assessment of heavy metal(loid)s in park soils of the largest megacity in China by using Monte Carlo simulation coupled with Positive matrix factorization model. *J Hazard Mater* 415, 125629. <https://doi.org/10.1016/j.jhazmat.2021.125629>.
- [15] Jackson, T.A., Telmer, K.H., Muir, D.C.G., 2013. Mass-dependent and mass-independent variations in the isotope composition of mercury in cores from lakes polluted by a smelter: Effects of smelter emissions, natural processes, and their interactions. *Chem Geol* 352, 27–46. <https://doi.org/10.1016/j.chemgeo.2013.05.036>.
- [16] Jiménez-Oyola, S., García-Martínez, M.J., Ortega, M.F., Bolonio, D., Rodríguez, C., Esbrí, J.M., et al., 2020. Multi-pathway human exposure risk assessment using Bayesian modeling at the historically largest mercury mining district. *Ecotoxicol Environ Saf* 201, 110833. <https://doi.org/10.1016/j.ecoenv.2020.110833>.
- [17] Kim, Y.G., Kwon, S.Y., Washburn, S.J., Hong, Y., Han, S.H., Lee, M., et al., 2024. Environmental forensics approach to source investigation in a mercury contaminated river: Insights from mercury stable isotopes. *J Hazard Mater* 461, 132559. <https://doi.org/10.1016/j.jhazmat.2023.132559>.
- [18] Li, P.Z., Lin, C.Y., Cheng, H.G., Duan, X.L., Lei, K., 2015. Contamination and health risks of soil heavy metals around a lead/zinc smelter in southwestern China. *Ecotoxicol Environ Saf* 113, 391–399. <https://doi.org/10.1016/j.ecoenv.2014.12.025>.
- [19] Li, Z.G., Feng, X.B., Li, G.H., Bi, X.Y., Sun, G.Y., Zhu, J.M., et al., 2011. Mercury and other metal and metalloids soil contamination near a Pb/Zn smelter in east Hunan province, China. *Appl Geochem* 26 (2), 160–166. <https://doi.org/10.1016/j.apgeochem.2010.11.014>.
- [20] Liang, L.C., Qiu, G.L., Chen, Z., 2015. Pollution characteristics and affecting factors of mercury in particulates PM<sub>2.5</sub> in Guiyang City. *Chin J Ecol* 34 (02), 510–515.
- [21] Lin, Y., Larssen, T., Vogt, R.D., Feng, X.B., 2010. Identification of fractions of mercury in water, soil and sediment from a typical Hg mining area in Wanshan, Guizhou province, China. *Appl Geochem* 25 (1), 60–68. <https://doi.org/10.1016/j.apgeochem.2009.10.001>.
- [22] Liu, B., Tian, K., He, Y., Hu, W.Y., Huang, B., Zhang, X.H., et al., 2022. Dominant roles of torrential floods and atmospheric deposition revealed by quantitative source apportionment of potentially toxic elements in agricultural soils around a historical mercury mine, Southwest China. *Ecotoxicol Environ Saf* 242, 113854. <https://doi.org/10.1016/j.ecoenv.2022.113854>.
- [23] Liu, M.D., 2019. Sources and fate of mercury in china's aquatic environment and human exposure to methylmercury through consumptions of aquatic products. Peking University.
- [24] Liu, M.D., Zhang, Q.R., Maavara, T., Liu, S.D., Wang, X.J., Raymond, P.A., 2021. Rivers as the largest source of mercury to coastal oceans worldwide. *Nat Geosci* 14 (9), 672. <https://doi.org/10.1038/s41561-021-00793-2>.
- [25] Mahaffey, K.R., Sunderland, E.M., Chan, H.M., Choi, A.L., Grandjean, P., Marien, K., et al., 2011. Balancing the benefits of n-3 polyunsaturated fatty acids and the risks of methylmercury exposure from fish consumption. *Nutr Rev* 69 (9), 493–508. <https://doi.org/10.1111/j.1753-4887.2011.00415.x>.
- [26] Mao, L.L., Ren, W.B., Liu, X.T., He, M.C., Lin, C.Y., Zhong, Y., et al., 2023. Tracking the multiple Hg sources in sediments in a typical river-lake basin by isotope compositions and mixing models. *J Hazard Mater* 459, 132166. <https://doi.org/10.1016/j.jhazmat.2023.132166>.
- [27] Niane, B., Guédron, S., Feder, F., Legros, S., Ngom, P.M., Moritz, R., 2019. Impact of recent artisanal small-scale gold mining in Senegal: Mercury and methylmercury contamination of terrestrial and aquatic ecosystems. *Sci Total Environ* 669, 185–193. <https://doi.org/10.1016/j.scitotenv.2019.03.108>.
- [28] Peng, D., Chen, M.Z., Su, X.Y., Liu, C.C., Zhang, Z.H., Middleton, B.A., et al., 2023. Mercury accumulation potential of aquatic plant species in West Dongting Lake, China. *Environ Pollut* 324, 121313. <https://doi.org/10.1016/j.envpol.2023.121313>.
- [29] Pratap, A., Mani, F.S., Prasad, S., 2020. Heavy metals contamination and risk assessment in sediments of Laucala Bay, Suva, Fiji. *Mar Pollut Bull* 156, 111238. <https://doi.org/10.1016/j.marpolbul.2020.111238>.
- [30] Qian, X.L., Wu, Y.G., Zhou, H.Y., Xu, X.H., Xu, Z.D., Shang, L.H., et al., 2018. Total mercury and methylmercury accumulation in wild plants grown at wastelands composed of mine tailings: Insights into potential candidates for phytoremediation. *Environ Pollut* 239, 757–767. <https://doi.org/10.1016/j.envpol.2018.04.105>.
- [31] Quintanilla-Villanueva, G.E., Villanueva-Rodríguez, M., Guzman-Mar, J.L., Torres-Gaytan, D.E., Hernandez-Ramirez, A., Orozco-Rivera, G., et al., 2020. Mobility and speciation of mercury in soils from a mining zone in Villa Hidalgo, SLP, Mexico: A preliminary risk assessment. *Appl Geochem* 122, 104746. <https://doi.org/10.1016/j.apgeochem.2020.104746>.
- [32] Sanga, T.R., Maseka, K.K., Ponraj, M., Tungaara, C., Mng'ong'o, M.E., Mwakalapa, E.B., 2023. Accumulation and distribution of mercury in agricultural soils, food crops and associated health risks: A case study of Shenda gold mine-Geita Tanzania. *Environ Chall* 11, 100697. <https://doi.org/10.1016/j.envc.2023.100697>.
- [33] Shahid, M., Dumat, C., Khalid, S., Schreck, E., Xiong, T.T., Niazi, N.K., 2017. Foliar heavy metal uptake, toxicity and detoxification in plants: a comparison of foliar and root metal uptake. *J Hazard Mater* 325, 36–58. <https://doi.org/10.1016/j.jhazmat.2016.11.063>.
- [34] Song, Z.C., Wang, C., Ding, L., Chen, M., Hu, Y.X., Li, P., et al., 2021. Soil mercury pollution caused by typical anthropogenic sources in China: Evidence from stable mercury isotope measurement and receptor model analysis. *J Clean Prod* 288, 125687. <https://doi.org/10.1016/j.jclepro.2020.125687>.
- [35] Sonke, J.E., Schäfer, J., Chmeleff, J., Audry, S., Blanc, G., Dupré, B., 2010. Sedimentary mercury stable isotope records of atmospheric and riverine pollution from two major European heavy metal refineries. *Chem Geol* 279 (3–4), 90–100. <https://doi.org/10.1016/j.chemgeo.2010.09.017>.
- [36] Sun, L.M., Zhang, X.D., Zheng, J.Y., Zheng, Y.Q., Yuan, D.X., Chen, W.J., 2021. Mercury concentration and isotopic composition on different atmospheric particles (PM<sub>10</sub> and PM<sub>2.5</sub>) in the subtropical coastal suburb of Xiamen Bay, Southern China. *Atmos Environ* 261, 118604. <https://doi.org/10.1016/j.atmosenv.2021.118604>.
- [37] US-EPA, 2017a. Mercury emissions: the global context. Agency USEP.
- [38] Voros, D., DiazSomoano, M., Gerslova, E., Sukorova, I., Suarez-Ruiz, I., 2018. Mercury contamination of stream sediments in the North Bohemian Coal District (Czech Republic): Mercury speciation and the role of organic matter. *Chemosphere* 211, 664–673. <https://doi.org/10.1016/j.chemosphere.2018.07.196>.
- [39] Wang, Q.R., Liu, R.M., Men, C., Xu, F., Guo, L.J., Shen, Z.Y., 2017. Spatial-temporal distribution and risk assessment of mercury in different fractions in surface sediments from the Yangtze River estuary. *Mar Pollut Bull* 124 (1), 488–495. <https://doi.org/10.1016/j.marpolbul.2017.07.034>.
- [40] Wang, X.Q., He, M.C., Xi, J.H., Lu, X.F., 2011. Antimony distribution and mobility in rivers around the world's largest antimony mine of Xikuangshan, Hunan Province, China. *Microchem J* 97 (1), 4–11. <https://doi.org/10.1016/j.microc.2010.05.011>.
- [41] Wang, Z.J., Zhang, G., Chen, X., Zhao, Q.J., Wang, W., Sheng, L.X., et al., 2019. Measurement and Scaling of Mercury on Soil and Air in a Historical Artisanal Gold Mining Area in Northeastern China. *Chin Geogr Sci* 29 (2), 245–257. <https://doi.org/10.1007/s11769-019-1026-2>.
- [42] Wen, B., Zhou, J.W., Tang, P.D., Jia, X.C., Zhou, W.Q., Huang, J.B., 2023. Antimony (Sb) isotopic signature in water systems from the world's largest Sb mine, central China: Novel insights to trace Sb source and mobilization. *J Hazard Mater* 446, 130622. <https://doi.org/10.1016/j.jhazmat.2022.130622>.
- [43] WHO, 2019. Mercury and health. World Health Organization. Accessed on September 16, 2019. <https://www.who.int/news-room/fact-sheets/detail/mercury-and-health>.
- [44] Xiao, H., Shahab, A., Xi, B.D., Chang, Q.X., You, S.H., Li, J.Y., et al., 2021. Heavy metal pollution, ecological risk, spatial distribution, and source identification in sediments of the Lijiang River, China. *Environ Pollut* 269, 116189. <https://doi.org/10.1016/j.envpol.2020.116189>.
- [45] Xu, X.H., Lin, Y., Meng, B., Feng, X.B., Xu, Z.D., Jiang, Y.P., et al., 2018. The impact of an abandoned mercury mine on the environment in the Xiushan region, Chongqing, southwestern China. *Appl Geochem* 88, 267–275. <https://doi.org/10.1016/j.apgeochem.2017.04.005>.
- [46] Yin, R.S., Feng, X.B., Wang, J.X., Li, P., Liu, J.L., Zhang, Y., et al., 2013. Mercury speciation and mercury isotope fractionation during ore roasting process and their implication to source identification of downstream sediment in the Wanshan mercury mining area, SW China. *Chem Geol* 336, 72–79. <https://doi.org/10.1016/j.chemgeo.2012.04.030>.
- [47] Yin, R.S., Feng, X.B., Chen, B.W., Zhang, J.J., Wang, W.X., Li, X.D., 2015. Identifying the sources and processes of mercury in subtropical estuarine and ocean sediments using Hg isotopic composition. *Environ Sci Technol* 49 (3), 1347–1355. <https://doi.org/10.1021/es504070y>.
- [48] Yin, X.B., Yao, C.X., Song, J., Li, Z.B., Zhang, C.B., Qian, W., et al., 2009. Mercury contamination in vicinity of secondary copper smelters in Fuyang, Zhejiang Province, China: Levels and contamination in topsoils. *Environ Pollut* 157 (6), 1787–1793. <https://doi.org/10.1016/j.envpol.2009.02.018>.
- [49] Yu, C.H., Liu, M.D., Guo, J.M., Lin, H.M., Yan, Y.Y., Zhang, Q.R., et al., 2022. Transport of mercury in a regulated high-sediment river and its input to marginal seas. *Water Res* 214, 118211. <https://doi.org/10.1016/j.watres.2022.118211>.
- [50] Zhang, W., Li, J.J., Qiu, H., Guo, X.Q., Fei, Z.J., Xing, Y., et al., 2024. Distribution and bioavailability of mercury in size-fractionated atmospheric particles around an ultra-low emission power plant in Southwest China. *J Environ Sci* 138, 141–152. <https://doi.org/10.1016/j.jes.2023.03.029>.
- [51] Zhang, Y.J., Sun, T., Ma, M., Wang, X., Xie, Q., Zhang, C., et al., 2022. Distribution of mercury and methylmercury in river water and sediment of typical manganese mining area. *J Environ Sci* 119, 11–22. <https://doi.org/10.1016/j.jes.2021.12.011>.
- [52] Zhao, B., O'Connor, D., Zhang, H., Jin, Y.L., Wang, Y.D., Yang, X.D., et al., 2023. Assessing mercury pollution at a primary ore site with both ancient and industrial mining and smelting activities. *Environ Pollut* 336, 122413. <https://doi.org/10.1016/j.envpol.2023.122413>.
- [53] Zheng, M.X., Feng, L., He, J.N., Chen, M., Zhang, J.W., Zhang, M.Y., et al., 2015. Delayed geochemical hazard: A tool for risk assessment of heavy metal polluted sites and case study. *J Hazard Mater* 287, 197–206. <https://doi.org/10.1016/j.jhazmat.2015.01.060>.
- [54] Zhong, M.R., Xiao, S.L., Zou, H., Zhang, Y.J., Song, Y., 2021. The effects of technical change on carbon intensity in China's non-ferrous metal industry. *Resour Policy* 73, 102226. <https://doi.org/10.1016/j.resourpol.2021.102226>.